Young's modulus determination of low-k porous films by wide-band DCC/LD LSAW*

Bai Maosen(白茂森)[†], Fu Xing(傅星), Dante Dorantes[†], Jin Baoyin(金宝印)
and Hu Xiaotang(胡小唐)

State Key Laboratory of Precision Measuring Technology and Instruments, School of Precision Instrument and Opto-Electronics
Engineering, Tianjin University, Tianjin 300072, China

Abstract: Low-k interconnection is one of the key concepts in the development of high-speed ultra-large-scale integrated (ULSI) circuits. To determine the Young's modulus of ultra thin, low hardness and fragile low-k porous films more accurately, a wideband differential confocal configured laser detected and laser-generated surface acoustic wave (DCC/LD LSAW) detection system is developed. Based on the light deflection sensitivity detection principle, with a novel differential confocal configuration, this DCC/LD LSAW system extends the traditional laser generated surface acoustic wave (LSAW) detection system's working frequency band, making the detected SAW signals less affected by the hard substrate and providing more information about the thin porous low-k film under test. Thus it has the ability to obtain more accurate measurement results. Its detecting principle is explained and a sample of porous silica film on Si (100) is tested. A procedure of fitting an experimental SAW dispersion curve with theoretical dispersion curves was carried out in the high frequency band newly achieved by the DCC/LD LSAW system. A comparison of the measurement results of the DCC/LD LSAW with those from the traditional LSAW shows that this newly developed DCC/LD LSAW can dramatically improve the Young's modulus measuring accuracy of such porous low-k films.

Key words: nano-porous low-k film; surface acoustic wave; differential confocal; Young's modulus; dispersion curve; wide band

1. Introduction

Inherent parasitic resistance-capacitance coupling has caused serious problems, such as signal propagation delay, crosstalk noise and high power dissipation, in high-speed ultra-large-scale integrated (ULSI) circuits[1]. Using a low-k material for the intra/inter layer dielectrics (ILDs) is one of the key solutions to mitigate these problems. According to the International Technology Road Map for Semiconductors (ITRS), dielectrics with $k < 2$ are required for the metallization interconnect system of the 45 nm ULSI technology node and beyond[1]. Nowadays, nanopores are introduced into dielectrics, such as silica, to decrease its k value by taking the advantage of the low k of air ($k = 1$). However, these nanopores deteriorate its mechanical properties dramatically, which causes problems for the integration of these porous films in processes such as chemical mechanical polishing (CMP)[1−3]. Thus, in situ, an accurate determination of the mechanical properties of low-k films is significant for the control of CMP and such metrology continues to be a critical part in the research and development of porous low-k materials[4].

The Young's modulus of low-k films is one of the key properties used to control CMP[3]. The present technologies to measure the Young's modulus include nanoindentation, surface Brillouin light scattering and laser-generated surface acoustic waves (LSAWs)[5−7]. Among all of these technologies,

the LSAW is favored for measuring the mechanical properties of such ultra thin (with thickness lower than 1 μm), soft (with Young's modulus within several GPa) and fragile (with nanopores) porous low-k dielectric films, because it is non-destructive, fast, accurate and is a promising in situ, in process measuring method used in the semiconductor industry[8].

The SAW's energy is almost concentrated within one or two wavelengths close to the surface, and decays exponentially as it goes into the body. The higher the frequency is, the more dramatically it decays[9]. In a layered structure, a lower frequency SAW is prone to be affected by the substrate, while higher frequency waves are almost dominated by the material properties close to the surface, which carries more information about the porous low-k film under test. Thus, to suppress the influence of the substrate, in order to obtain more accurate mechanical properties of the porous films, or even to investigate "higher order" propagating surface

Sezawa modes with different velocities in layered materials, it is essential to improve the bandwidth of the measuring system to detect the high frequency SAW[10]. Sorted by their detection principle, there are usually three kinds of LSAW technologies: the first type is based on light interference; the second type is based on piezoelectric transduction i.e. PZT LSAWs; and the third type is based on light deflection sensitivity detection. The first type of LSAW always has a limited responding frequency band[11]. Until now, the PZT LSAW was

---

† Corresponding author. Email: baimaosen@tju.edu.cn; dorantes@tju.edu.cn
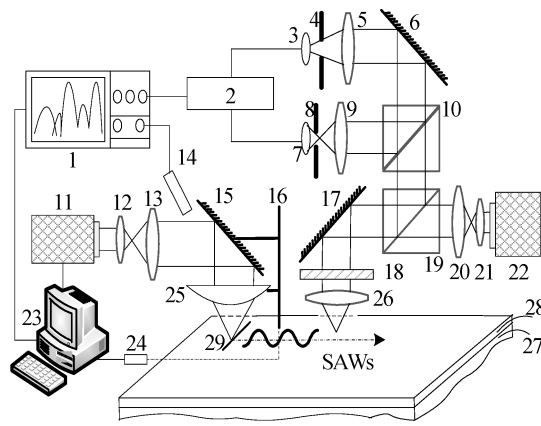
1: Oscilloscope; 2: Subtracter; 3,7: Optoelectronic sensor;
4,8: Pin hole; 5,9: Collecting lens; 6,15,17: Mirrors;
10: Beam splitter; 11: Pulse laser; 12,13,20,21: Extenders;
14: Photodiode; 16: Device support; 18: Quarter-wave plate;
19: Polarized beam splitter; 22: He-Ne laser; 23: Central computer;
24: Motor driver; 25: Cylindrical lens; 26: Object lens;
27: Film; 28: Substrate; 29: Line of laser pulse

Fig. 1. Set-up of DCC/LD LSAW system.

Fig. 2. Principle of DCC/LD LSAW detection. (a) Without SAW. (b) With SAW.

the most successful LSAW[7, 8, 12, 13]. However, it is a contact detecting method, in which it is easy to introduce contamination to the film under test and it also has a frequency band lower than 120 MHz[7, 8, 13]. A light deflecting sensitivity based LSAW inherently has the fastest responding ability and has the widest frequency band, however it is prone to be affected by environmental noise and fluctuations of its detecting laser beam[14].

This paper strengthens the LSAW's ability to determine low-*k* porous films' Young's modulus more accurately by extending its bandwidth by a newly developed differential confocal configured laser detected and laser-generated surface acoustic wave (DCC/LD LSAW) technology, which is based on the principle of light deflection sensitivity detection. While it inherits the advantages of fast response and non-contact detection of such deflection sensitivity detection systems, with a novel differential confocal configuration, this DCC/LD LSAW system successfully suppresses environmental common model noises and wipes off high frequency disturbances caused by the detecting laser's power fluctuation. Using this system, a sample of porous silica film on Si (100) substrate was tested. High frequency SAWs that had not been acquired previously by other techniques are now obtained by this DCC/LD LSAW system. Owing to the good quality of the high frequency SAW, a fitting of the experimental dispersion curve with theoretical curves can be carried out for such high frequency bands, which yields a more accurate determination result of the low-*k* film's Young's modulus.

2. Experiment system

Figure 1 shows the schematic of the constructed DCC/LD LSAW system.

In the experiment, the SAWs are generated by a laser pulse that is focused into a line on the sample's surface by a cylindrical lens. As the SAWs propagate, they cause disturbances at the detecting point on the surface, which causes a slight ro-

tation of the reflecting angle of the detecting beam that comes from a continuous He–Ne laser of 10 mW. This detecting beam is focused onto the surface by the object lens and its reflected beam is collected by the same lens since it shares the focal plane of the incident beam. The reflected beam is then split half by half by a beam splitter. Two identical optoelectronic sensors are differentially configured to detect the variation of the reflected detecting beams. One is placed before the focal plane of its collecting lenses and the other is placed behind its collecting lenses' focal plane. Therefore, if there is a slight variation of the reflecting angle at the detecting point caused by the SAW, the illuminating power received by one sensor increases, while the other decreases. The absolute value of the subtracter's output increases. Noises such as the intrinsic drift of the detecting laser and the convection of the light-transmitting medium are eliminated as common mode components by the differential configuration. The confocal optical detection principle ensures the quick response and high spatial resolution of the detection system, while the differential configuration of the two sensors increases the signal productivity and keeps the signal immune from noises.

Before the experiment, devices on the detecting beam path should be adjusted so that the differential output is zero. As SAWs propagate to the detecting point, the reflecting angle varies slightly, which leads to the unbalance of the receiving light power of the two optoelectronic sensors, and then the output signal of the subtracter varies. Therefore, the SAWs on the sample surface are detected.

3. Detection principle

In this DCC/LD LSAW system, a continuous laser light provided by a He–Ne laser is used as the detecting light. Its power is of the Gauss distribution type. If there is no disturbance of acoustic waves on the illuminated surface, as shown in Fig. 2(a), the reflected light almost shares the same path as the incident light and the peak of the Gauss distribution is at the centre of the inducing area of the optoelectronic sensor. As the illuminated surface is disturbed by the acoustic waves, as

shown in Fig. 2(b), the micro particle on the illuminated point of the surface is rotated by a small angle, ϕ, which causes the power distribution centre of the reflected light to shift a distance Δx from the origin, i.e. the centre of the spot of the reflected light also shifts a distance Δx from the centre of the inducing area of the optoelectronic sensor. By splitting the reflected light half by half by two identical optoelectronic sensors in a differential configuration, one sensor has a distance shift of Δx and the other has a shift of $-\Delta x$, i.e. a shift towards the opposite direction.

Given this differential confocal configuration, we can set M_0 as the productivity of the optoelectronic sensor and P_0, P_1 as the power received by the two identical sensors, respectively. Then we can get the differential output of the two identical sensors as

$$\Delta V = M_0(P_1 - P_2). \tag{1}$$

As ϕ is relatively far smaller than d in orders of magnitude under the standard international unit (d is the distance between the lens and the illuminated surface), the shifted distance Δx can be expressed as

$$\Delta x = \phi d. \tag{2}$$

Thus, the power for the Gauss distributed light received by the two optoelectronic sensors can be written as follows, respectively:

$$P_1 = \frac{2}{\pi a^2} \iint_{s_1} P_0 e^{-2[(x-\Delta x)^2 + y^2]/a^2} \mathrm{d}x \mathrm{d}y, \tag{3}$$

$$P_2 = \frac{2}{\pi a^2} \iint_{s_2} P_0 e^{-2[(x-\Delta x)^2 + y^2]/a^2} \mathrm{d}x \mathrm{d}y, \tag{4}$$

where P_0 represents the power of the incident light, a stands for the radius of light spot on the inducing area of the optoelectronic sensor and s_1, s_2 are the total areas of the induced fields of the two sensors, respectively. As a is far smaller than the radius of the sensor inducing field, the boundary of the integrals in Eqs. (3) and (4), which represents the boundary of the sensor inducing field, can be viewed as infinite and then getting:

$$
\begin{aligned}
P_1 &= \frac{2}{\pi a^2} P_0 \int_{-\infty}^{+\infty} \exp\frac{-2y^2}{a^2}\mathrm{d}y \int_{0}^{+\infty} \exp\frac{-2(x-\Delta x)^2}{a^2}\mathrm{d}x \\
&= \frac{2P_0}{\sqrt{2\pi}a} \int_{-\Delta x}^{\infty} \exp\left(-\frac{2x'^2}{a^2}\right)\mathrm{d}x',
\end{aligned}
\tag{5}
$$

$$
\begin{aligned}
P_2 &= \frac{2}{\pi a^2} P_0 \int_{-\infty}^{+\infty} \exp\frac{-2y^2}{a^2}\mathrm{d}y \int_{-\infty}^{0} \exp\frac{-2(x-\Delta x)^2}{a^2}\mathrm{d}x \\
&= \frac{2P_0}{\sqrt{2\pi}a} \int_{-\infty}^{-\Delta x} \exp\left(-\frac{2x'^2}{a^2}\right)\mathrm{d}x',
\end{aligned}
\tag{6}
$$

where $x' = x - \Delta x$. Then the differential output of the two identical optoelectronic sensors is:

$$\Delta V = M_0(P_1 - P_2) = \frac{2}{\sqrt{2\pi}a} P_0 M_0 \int_{-\Delta x}^{\Delta x} \exp\left(-\frac{2x'^2}{a^2}\right)\mathrm{d}x'. \tag{7}$$

As the shift Δx is far smaller than the radius of the light spot on the inducing area of the optoelectronic sensor, then we get

$$\Delta V = \frac{4P_0 M_0}{\sqrt{2\pi}a}\Delta x. \tag{8}$$

From the relationship between the radius of a Gauss light spot and its propagating distance, we have

$$a = \frac{\lambda \mathrm{d}}{\pi a_0}, \tag{9}$$

where λ is the wavelength of the light in its transmitting media. Taking Eqs. (2) and (9) into Eq. (8) yields

$$\Delta V = \frac{4V_0}{\sqrt{2\pi}} \frac{\pi a_0}{\lambda}\phi. \tag{10}$$

Given a wave with an angular frequency of ω_a, propagating along x, its displacements can be expressed as

$$u = u_a \cos(\omega_a t + k_a x), \tag{11}$$

in which u_a is the amplitude of the wave and k_a is its propagating constant. As ϕ is very small,

$$\phi = \frac{\partial u}{\partial x} = k_a u_a \sin(\omega_a t - k_a x) = \frac{k_a}{\omega_a}\frac{\partial u}{\partial t}. \tag{12}$$

Substituting Eq. (12) in Eq. (10), we get

$$\Delta V = \frac{4V_0}{\sqrt{2\pi}} \frac{\pi a_0}{\lambda} \frac{k_a}{\omega_a} \frac{\partial u}{\partial t}, \tag{13}$$

thus it can be concluded that the differential output of the two identical optoelectronic sensors contains the necessary information about the particle's vibration velocity caused by the SAW.

4. Theoretical solution

The SAWs get dispersed as they propagate on the surface of a layered structure. Two theoretical models exist for the calculation of theoretical dispersion curves: one is the isotropic film/substrate model, as shown in Fig. 3(a); the other is the transverse-isotropic film/substrate model. The former views the film as isotropic, which is an approximation and only suitable for compact film or for low-k film with disorderly-distributed pores[7, 8, 12, 13]. Research reports have found that the shape and distribution type of nanopores in dielectric films must be tightly controlled to obtain a sufficient mechanical strength for the elimination of cracks and delamination during CMP[2, 15, 16]. It has been proved theoretically and experimentally that dielectric films with periodically distributed nanopores can gain much better mechanical properties[15, 16]. Until now, with self-assembly technology, periodic hexagonal porous silica film has been developed successfully[17−20]. Its theoretical periodic model is also described in Ref. [20]. For such a periodic porous low-k film, the isotropic film/substrate model is no longer suitable and the newly transverse-isotropic film/substrate model is established, as is described in Refs. [21, 22]. In this paper, for the experimental sample of periodic porous silica film deposited on Si(100) with self-assembly

(a) Isotropic film/substrate model

(b) Transverse-isotropic film/substrate model
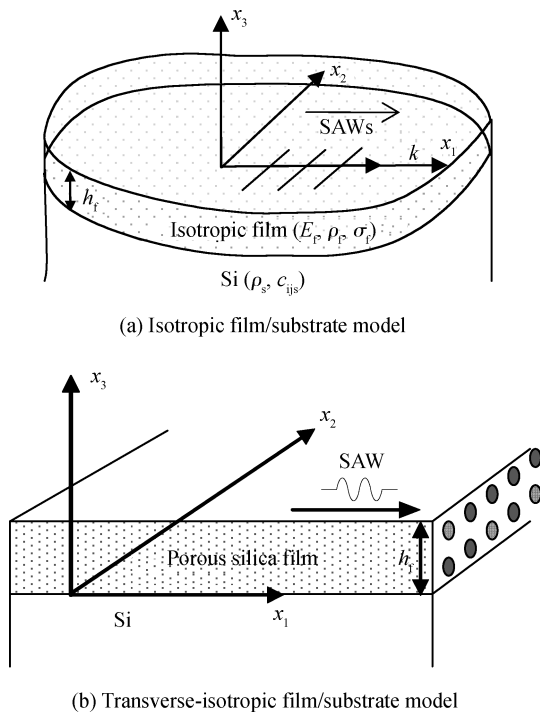
Fig. 3. Theoretical dispersion curves calculation model for SAW propagation in a film/Si substrate layered structure.

Table 1. Parameters of the porous silica film/Si substrate sample under test.

Parameter	Film	Substrate
Type	Periodic porous silica film	Intrinsic Si(100)
Wafer size (inch)	—	2
Thickness (μm)	0.223	450
Nanopores' direction	Si [100]	—
Porosity	0.33	—
Density (kg/m^3)	1130	2300
Poisson rate	0.202	0.27

technology, the advanced model of the transverse-isotropic film/substrate model is adopted to calculate its theoretical dispersion curves.

5. Results and discussion

As porous low-*k* silica film is one of the most promising ILDs in interconnection in ULSI, a sample of periodic porous silica film on Si(100) substrate is tested in this paper. Table 1 gives a detailed description of the sample under test. The porous silica film is developed by self-assembly technology, with its nanopores lying periodically in the direction of Si [100][17]. The film's *k* value is measured by capacitance measurement technology as 2.3; its density is measured by X-ray reflectance; and its thickness is determined by spectrumscopic ellipsometry; its porosity was measured by the ellipso–porosimetry technique.

As explained before, this periodic porous sample is treated as a transversely isotropic structure in a theoretical SAW dispersion curve calculation. Its calculation model is established as shown by Fig. 3(b). Concrete calculation procedures have
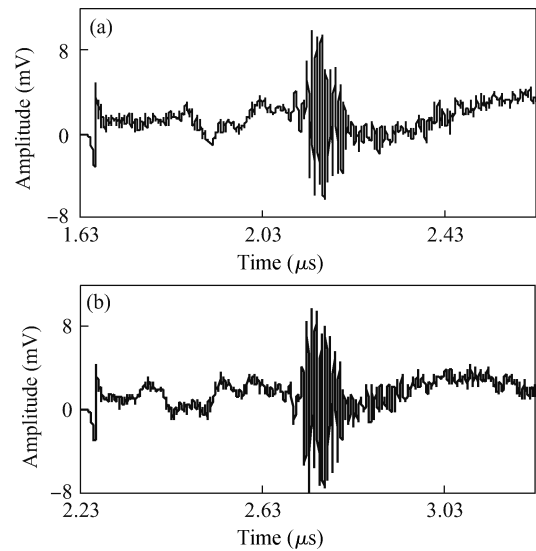
Fig. 4. SAW signals detected at position (a) d_1 and (b) d_2 by DCC/LD LSAW for periodic porous silica film on Si(100).

been described in detail in Refs. [21, 22]. The parameters used in the theoretical calculation are set according to Table 1. Its Young's modulus is pre-set within the range of 0.90–1.40 GPa, with an increasing step of 0.01 GPa during the calculation. Theoretically calculated dispersion curves for this low-*k* film under test in a low frequency band (40–140 MHz) and in a high frequency band (250–330 MHz) are shown by dashed lines in Figs. 6(a) and 6(b), respectively.

In the experiment, SAWs propagate along the Si [110] direction. To calculate its dispersion curve, signals at positions d_1 and d_2 are detected, as shown in Figs. 4(a) and 4(b), respectively. The distance between the two detected points is $|d_1 - d_2|$ = 3 mm. The SAWs last for about 1 μs. As the energy of the SAW is almost confined at the surface of the sample within one or two wavelengths and decays exponentially within its perpendicular depth, the higher the SAW's frequency, the more dramatically it disperses. So the significant basic waveform similarity and the varied details of the SAW signals detected at the two probe points verified their effectiveness.

The amplitude spectrum of the SAW signal was obtained by FFT and is shown by Fig. 5(a). Before FFT, the DC components of the signal are filtered out because they have no relationship with SAW dispersion analysis, while they contain a large part of the energy of the SAW signal.

To verify the functionality of this newly developed DCC/LD LSAW, or even to prove its ability to extend the traditional LSAW's bandwidth and thus to show that it achieves a higher Young's modulus measuring accuracy for such periodic porous low-*k* film, a test for the same sample by piezoelectric LSAW (PZT LSAW, which is the most successful traditional LSAW until now[7, 8, 12, 13].) was also carried out in this paper. Figure 5(b) shows the amplitude spectrum obtained by PZT LSAW. Comparing Fig. 5(a) and Fig. 5(b), it can be easily found that the only useful frequency band for PZT LSAW is 50–120 MHz, as has been reported before[7, 8, 12, 13]; while this newly developed DCC/LD LSAW not only obtains a high quality SAW signal in the traditional frequency band of 50–120 MHz, but also in the high frequency band of 250–320
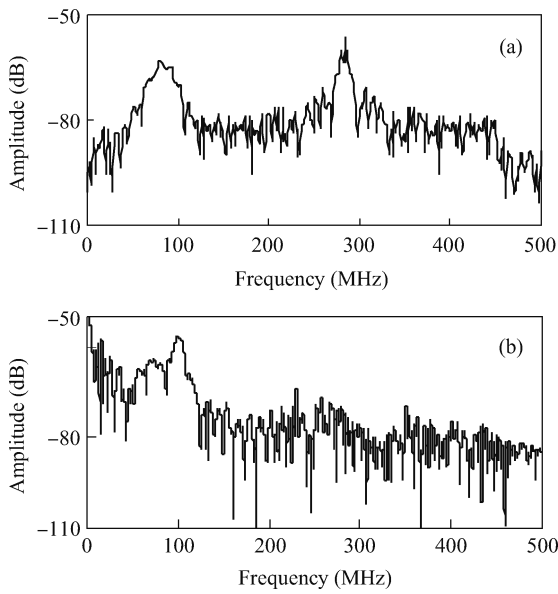
Fig. 5. Comparison of SAW signals' amplitude spectra obtained by (a) DCC/LD LSAW and (b) PZT LSAW for periodic porous silica film on Si(100).

MHz, which has not been achieved by any other LSAW before.

The LSAW determines the film's Young's modulus by fitting the experimental dispersion curve with theoretical dispersion curves[7, 8, 10, 12, 13]. The experimental dispersion curves are calculated by Eq. (14).

$$c(f) = \frac{2\pi f(d_2 - d_1)}{\Phi_2(f) - \Phi_1(f)}. \tag{14}$$

$\Phi_1(f)$ and $\Phi_2(f)$ in Eq. (14) represent the phase spectrums of the two detected signals in the experiment, respectively. The calculation results are shown in Fig. 6. The solid line in Fig. 6(a) shows the experimental dispersion curve obtained by PZT LSAW; while the solid line in Fig. 6(b) shows the experimental dispersion curve obtained by DCC/LD LSAW. The dashed lines in both Figs. 6(a) and 6(b) show the theoretical dispersion curves calculated as explained before.

Figures 6(a) and 6(b) show the comparison of the fitting results of the experimental dispersion curve with the theoretical curves in PZT LSAW and in this new DCC/LD LSAW, respectively. As SAWs get more dispersed in a higher frequency band than in a lower frequency band, the dispersion curves in a higher frequency band are more distinguishable, as is seen in Figs. 6(a) and 6(b). Thus fitting the experimental curve with theoretical curves in a higher frequency band can increase the measuring accuracy approximately. In Fig. 6(a), since the useful frequency band for PZT LSAW is only of 50–120 MHz, the dispersion curves' fitting procedure can only be carried out in such a low frequency band. Thus with an accuracy of 0.1 GPa, it can only narrowly distinguish which theoretical curve fits the experimental dispersion curve best, as can be seen in Fig. 6(a). As for this newly developed DCC/LD LSAW, owing to the SAW's good quality in a high frequency band of 250–320 MHz, its dispersion curves' fitting procedure can be performed in the newly achieved high frequency band. With the theoretical curves' higher separation degree in such a frequency band, it is safe to say that a theoretical curve of
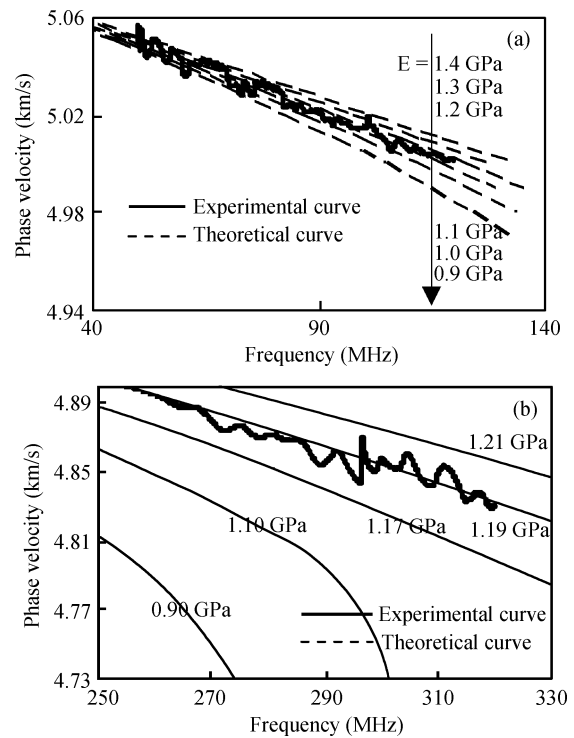
Fig. 6. Fitting experimental dispersion curve with theoretical curves in (a) PZT LSAW and (b) DCC/LD LSAW for periodic porous silica film on Si(100).

Table 2. Measurement results of porous silica film/Si(100) sample under test.

Testing method	DCC/LD LSAW	PZT LSAW	Nanoindentation
Testing points	10	10	4
Fitting frequency band (MHz)	250–320	50–120	—
Average Young's modulus (GPa)	1.19	1.1	3.83
Standard deviation (GPa)	0.0126	0.0789	0.4918
Measuring accuracy (GPa)	0.02	0.1	0.06

1.19 GPa fits the experimental dispersion curve best, with an accuracy of 0.02 GPa, as is shown by Fig. 6(b).

Table 2 lists the measurement results for the periodic porous silica film/Si(100) sample by PZT LSAW and DCC/LD LSAW. To verify their functionality, the same sample was also tested by nanoindentation. That measurement result is also given in Table 2. As reported before[23], since it is affected by the hard substrate, the nanoindentation testing result is much higher than that of DCC/LD LSAW and PZT LSAW. However, the test results of DCC/LD LSAW and PZT LSAW keep reasonably consistent with each other, which verified the functionality of the newly developed DCC/LD LSAW system. Due to its ability to achieve a high frequency SAW signal with good quality, this novel DCC/LD LSAW improves the measurement accuracy for such porous low-k film up to 0.02 GPa, as is shown in Table 2.

6. Conclusions

A DCC/LD LSAW detection system was developed. As this system is based on the deflection-sensitivity detection principle, it has an ultra fast response and a high deflection sensitivity, which are of great advantage in the detection of high frequency SAW signals. By a novel differential confocal configuration, this system successfully suppressed high frequency disturbances in such a deflection-sensitivity detection system and obtained high frequency SAW signals that had not been achieved before with good quality. Theoretical dispersion curves for such periodic nano-porous low-k film are calculated using the transverse-isotropic film/substrate model, which has been established before. Comparison tests of DCC/LD LSAW and PZT LSAW for this same porous silica film/Si(100) sample were carried out, and the results show that this newly developed DCC/LD LSAW can obtain good quality high frequency SAW signals that have not been achieved before. Thus it could take advantage of the SAW dispersion curves' higher distinguishability in the higher frequency band. The dispersion curves' fitting procedure of DCC/LD LSAW was conducted in the newly gained high frequency band, which dramatically improved the Young's modulus' measurement accuracy for such porous low-k film.

Acknowledgments

References

[1] International technology roadmap for semiconductors. Interconnect, Semiconductor Industry Association, 2007

[2] Kondo S, Tokitoh S, Yoon B U, et al. Low-pressure CMP for reliable porous low-k/Cu integration. Proceedings of IIT C, 2003: 86

[3] Jin C, Lin S, Wetzel J T. Evaluation of ultra-low-k dielectric materials for advanced interconnects. J Electron Mater, 2001, 30(4): 284

[4] The international technology roadmap for semiconductors. Interconnection, Semiconductor Industry Association, 2009

[5] Passeri D, Bettucci A, Germano M, et al. Local indentation modulus characterization via two contact resonance frequencies atomic force acoustic microscopy. Microelectron Eng, 2007, 84(3): 490

[6] Shintani K, Yanagitani T, Matsukawa M, et al. Non-destructive evaluation of thin ZnO shear wave transducer by Brillouin scattering. IEEE International Ultrasonics, Ferroelectrics, and Frequency Control Joint, 50th Anniversary Conference, 2004: 1864

[7] Flannery C M, Murray C, Streiter I, et al. Characterization of thin-film aerogel porosity and stiffness with laser-generated surface acoustic waves. Thin Solid Films, 2001, 388(1): 1

[8] Xiao X, Hata N, Yamada K, et al. Mechanical property determination of thin porous low-k films by twin-transducer laser generated surface acoustic waves. Jpn J Appl Phys, 2004, 43(2): 508

[9] Farnell G W, Adler E L. Physical acoustics. New York: Academic Press, 1972

[10] Côte R, van der Donck T, Celis J P, et al. Surface acoustic wave characterization of a thin, rough polymer film. Thin Solid Films, 2009, 517(8): 2697

[11] Ma X Q, Mizutani Y, Takemoto M. Laser-induced surface acoustic waves for evaluation of elastic stiffness of plasma sprayed materials. J Mater Sci, 2001, 36: 5633

[12] Schneider D, Schwarz T, Scheibe H J, et al. Non-destructive evaluation of diamond and diamond-like carbon films by laser induced surface acoustic waves. Thin Solid Films, 1997, 295(1/2): 107

[13] Vaz F, Carvalho S, Rebouta L, et al. Young's modulus of (Ti,Si)N films by surface acoustic waves and indentation techniques. Thin Solid Films, 2002, 408(1/2): 160

[14] Monchalin J P. Optical detection of ultrasound. IEEE Trans Ultrasonics, Ferroelectrics, and Frequency Control, UFFC-33, 1986, 5: 485

[15] Chen J Y, Pan F M, Cho A T, et al. Microstructure and mechanical properties of surfactant templated nanoporous silica thin films: effect of methylsilylation. J Electronchem Soc, 2003, 150: 123

[16] Guliants V V, Carreon M A, Lin Y S. Ordered mesoporous and macroporous inorganic films and membranes. Journal of Membrane Science, 2004, 235: 53

[17] Kikkawa T, Oku Y, Kohmura K, et al. A scalable low-k/Cu interconnect technology using self-assembled ultra-low-k porous silica films. IEEE 7th ICSICT, Beijing, 2004, (1/2/3): 493

[18] Oku Y, Yamada K, Goto T, et al. Novel self-assembled ultra-low-k porous silica films with mechanical strength for 45 nm BEOL technology. IEDM, 2003: 6.1.3

[19] Kikkawa T, Kuroki S, Sakamoto S, et al. Influence of humidity on electrical characteristics of self-assembled porous silica low-k films. J Electrochem Soc, 2005, 152(7): G560

[20] Hidenori M, Hisanori M, Hirofumi T, et al. Theoretical investigation of dielectric constant and elastic modulus of two-dimensional periodic porous silica films with elliptical cylindrical pores. Jpn J Appl Phys, 2005, 44(3): 1161

[21] Bai M S, Xiao X, Li Z G, et al. Investigation of SAWs propagating on the nano-porous film. 8th International Conference on Solid-State and Integrated Circuit Technology, 2006: 1456

[22] Li Zhiguo, Yao Suying, Xiao Xia, et al. A model for mechanical property evaluation of the periodic porous low-k materials by SAW. Chinese Journal of Semiconductors, 2007, 28(11): 1722

[23] Mogilnikov K P, Baklanov M R. Determination of Young's modulus of porous low-k films by ellipsometric porosimetry. Electrochem Solid-State Lett, 2002, 5(12): 29